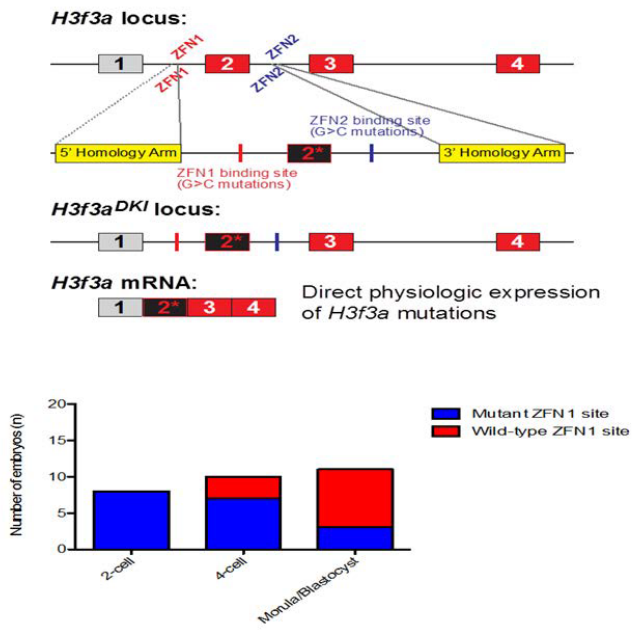
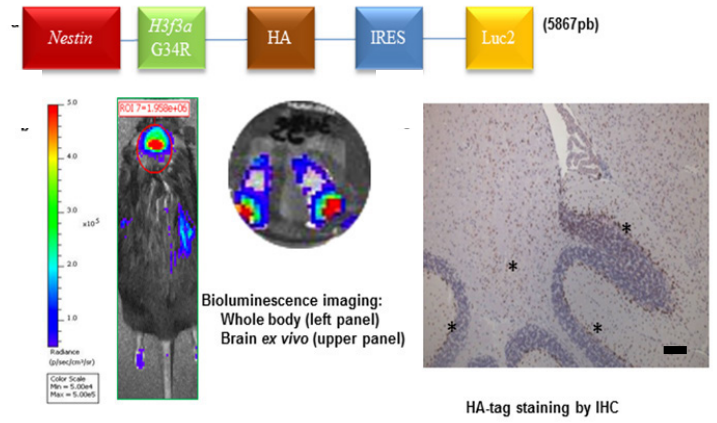


A



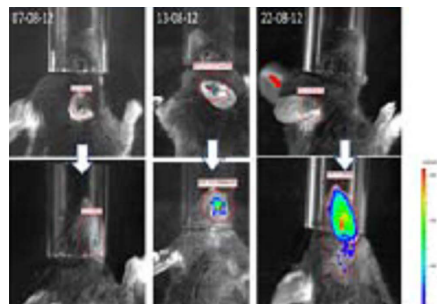
B



C

Background	Vector 1	Vector 2	Vector 3	Vector 4	Ratio	Total DNA (µg)	Age/hour
C57Bl/6	SB13/fluc	Pt2-H3.3K27M-HA	—	—	1:1	1	≤48
		Pt2-EV-HA	—	—	1:1	1	≤48
		Pt2-H3.3K27M-HA	shp53/GFP	—	1:1:1	1.5	≤48
		Pt2-H3.3K27M-HA	shp53/GFP	—	1:1:1	1	≤48
		Pt2-EV-HA	shp53/GFP	—	1:1:1	1.5	≤48
		NRAS-G12V	SV40-LgT	—	1:2:2	0.5	≤48
		Pt2-H3.3K27M-HA	NRAS-G12V	—	1:2:2	1	≤48
		Pt2-H3.3K27M-HA	shp53/GFP	shATTRX/GFP	1:1:1:1	1	≤48

D



E

Background	Sleeping beauty mice	Number	Hydrocephalus	Proliferating cluster cells	Age
C57Bl/6	SB13/fluc Pt2-H3.3K27M-HA	24	8 (33%)	0	one year
	SB13/fluc Pt2-H3.3K27M-HA-shp53/GFP	23	10 (43%)	2 (15%)	one year
	SB13/fluc Pt2-H3.3K27M-HA-NRAS-G12V	5	1 (20%)	2 (50%)	one year
	SB13/fluc Pt2-H3.3K27M-HA-shp53-shATTRX/GFP	13	7 (53%)	2 (33%)	9 months
	SB13/fluc shp53/GFP	6	1 (16%)	0	one year
	SB13/fluc NRAS-G12V-SV40-LgT	5	1 (20%)	3 tumors	4w-4months
	SB13/fluc Pt2 EV	18	6 (33%)	0	one year

Figure S1. Related to Figure 1. H3.3^{K27M} expression is embryonic lethal, while targeted expression via the *Nes* promoter or in postnatal animals fails to induce tumorigenesis.

(A) Schematic describing strategy for engineering knock-ins of H3.3 mutations. Zinc finger nuclease (ZFN1 and ZFN2)-mediated targeting of the endogenous mouse *H3f3a* locus and allelic replacement mediates the exchange of the wild-type exon 2 with an exon 2 harboring K27M or G34R mutations, and introduces ZFN1 and ZFN2 G>C binding site mutations to prevent re-excision. Bar graph below shows number of FVB/N-C57BL6 hybrid embryos with ZFN-mediated double knock-in of K27M reaching the morula/blastocyst stage, compared to WT embryos. Genomic DNA from embryos at 2-cell, 4-cell and morula blastocyst stages was sequenced for ZFN1 G>C binding site mutations.

(B) Schematic describing targeting of mutant H3.3^{HA} (G34R or K27M) and luciferase expression downstream of the NPC-specific *Nes* promoter in mice. Detection of luciferase activity and nuclear HA *in vivo*. Scale bar represents 100 μm .

(C) Summary of neonatal injections carried out with different combinations of Sleeping Beauty transposable vectors, their respective ratios and DNA concentrations. All experiments used SB13/fluc transposase and mice \leq 48 hours old. EV-HA was used as negative control and NRAS-G12V + SV40-LgT were used as positive controls.

(D) Demonstration of bioluminescence *in vivo* following injection of luciferase-encoding Sleeping Beauty transposable vectors and intraperitoneal luciferin administration.

(E) Results of neonatal transduction using Sleeping Beauty transposons. NRAS-G12V + SV40-LgT was used as a positive control.

Table S1. Related to Figures 1, 2, 3 and 6. Summary of tumor penetrance at different timepoints and histological features.

Condition	Location	Tumor at 4-6 mo.	Tumor at 8-11 mo.	Penetrance	Total n	Tumor features		
						Diffuse	Focal and diffuse	Nectrotic foci
EV control	cortex	0	0	0	3			
WT control	cortex	0	0	0	4			
G34R control	cortex	0	0	0	7			
K27M control	cortex	few Ki67+ cells, dispersed	few Ki67+ cells, dispersed	0	3			
WT-P	hindbrain	0	0	0	3			
G34R-P	hindbrain	0	0	0	2			
K27M-P	hindbrain	3	undetermined	N/A	3	0	3	0
K27M-P	cortex	2	5	100%	7	7	0	0
EV-AP	cortex	0	0	0	11			
WT-AP	cortex	0	0	0	8			
G34R-AP	cortex	0	0	0	11			
K27M-AP	cortex	11	6	100%	17	6	11	0
EV-PDGFRA control	cortex	0	undetermined	N/A	4			
EV-APP	cortex	1	2	25%	12			
WT-APP	cortex	1	0	10%	10			
G34R-APP	cortex	0	2	18%	11			
K27M-APP	cortex	11	6	100%	17	0	17	6
EV-APD842V	cortex	5	undetermined	100%	5	0	5	5
WT-APD842V	cortex	5	undetermined	100%	5	0	5	5
G34R-APD842V	cortex	5	undetermined	100%	5	0	5	5
K27M-APD842V	cortex	5	undetermined	100%	5	0	5	5

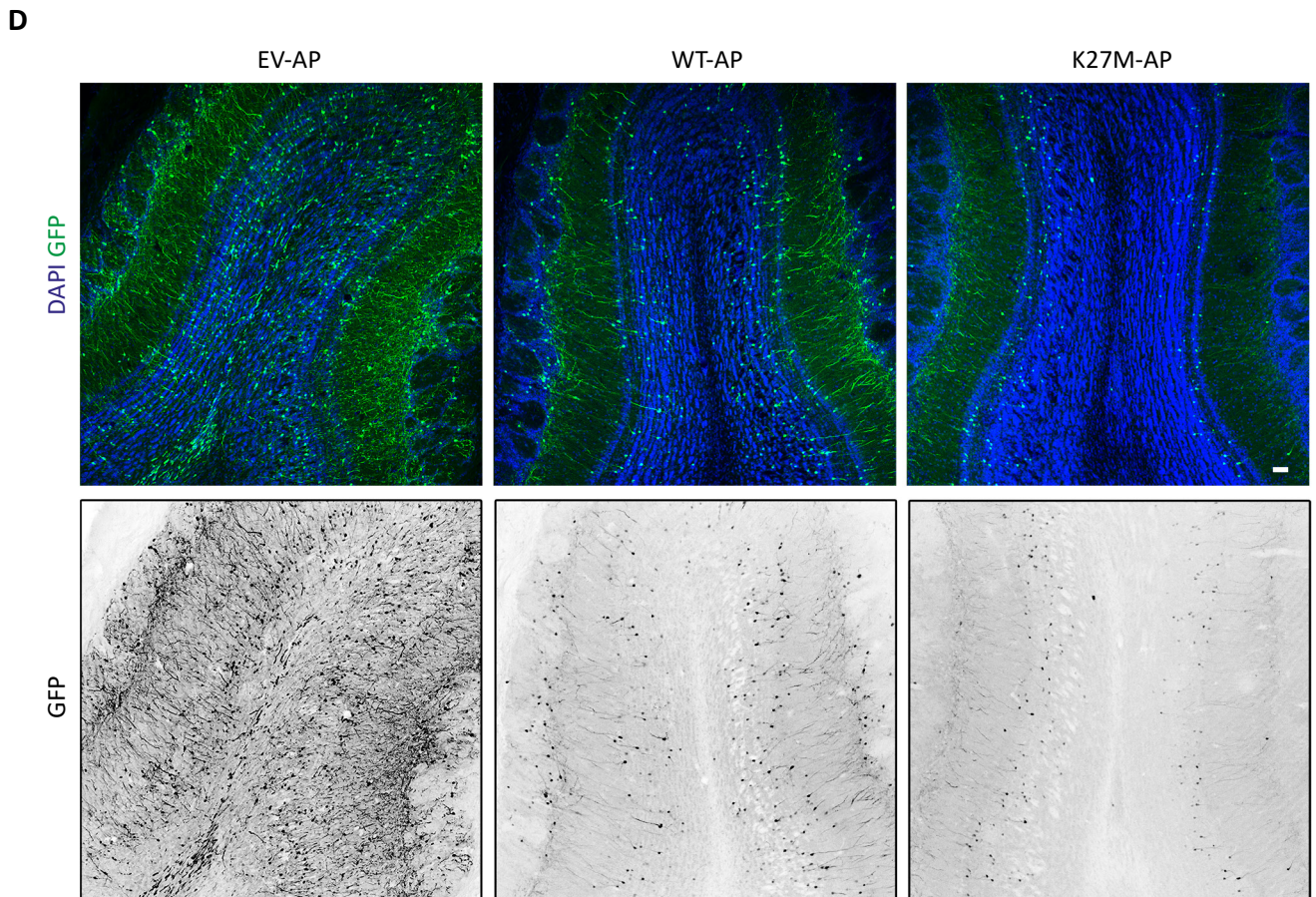
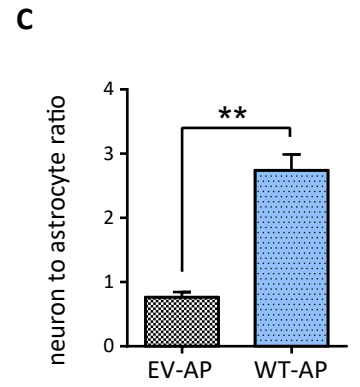
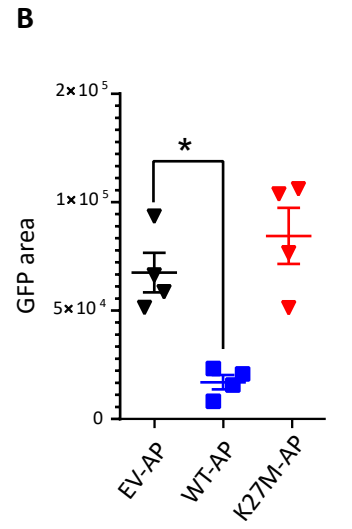
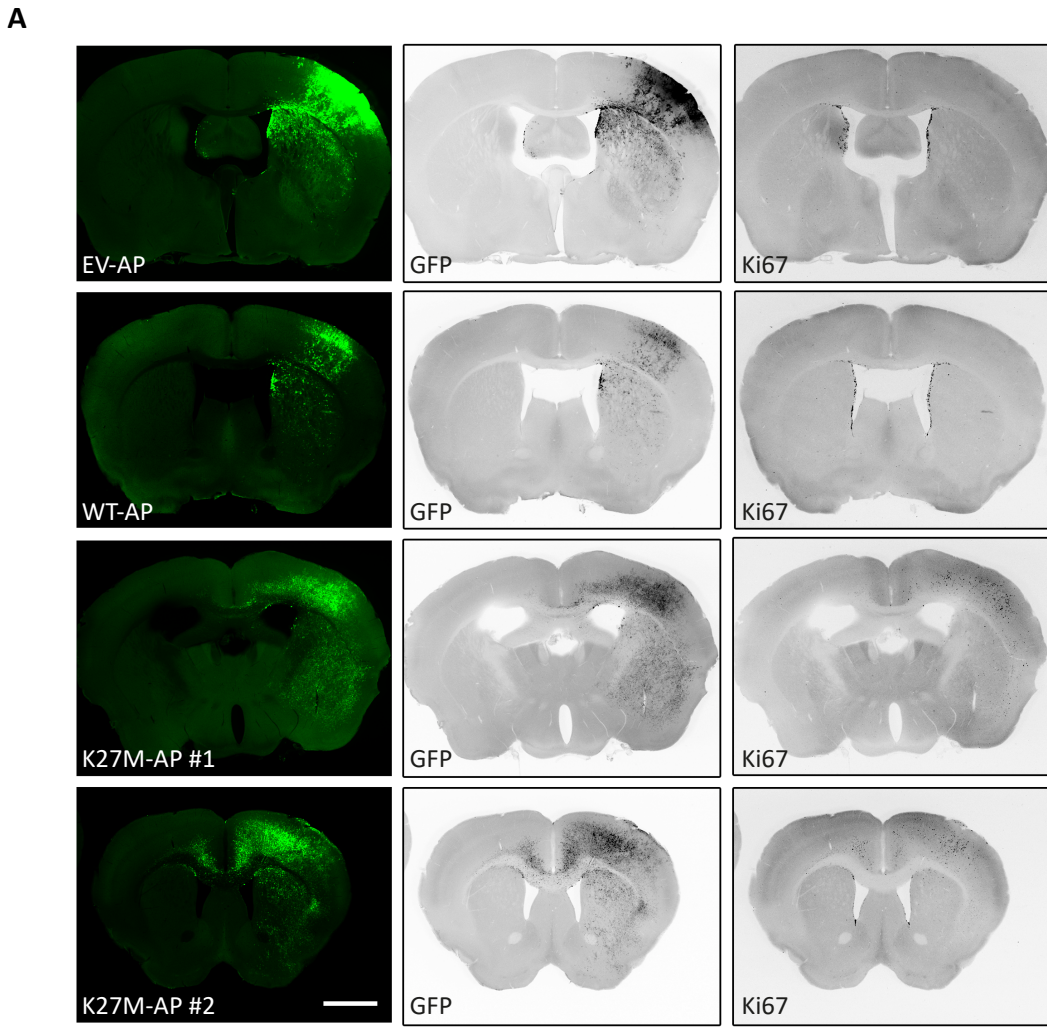


Figure S2. Related to Figure 2. K27M-AP tumor cells migrate ventrally and/or contralaterally and reduce ongoing postnatal neurogenesis. (A) Coronal sections demonstrating GFP⁺ signal in EV-AP, WT-AP and two different biological replicates of K27M-AP brains 4 months following surgery. Scale bars represent 1.5 mm. **(B)** Quantification of total GFP⁺ area in EV-AP, WT-AP and K27M-AP coronal sections. Data are represented as mean \pm SEM. **(C)** Neuron-to-astrocyte ratio in WT-AP compared to EV-AP. Data are represented as mean \pm SEM. **(D)** Representative examples of number of subventricular zone (SVZ)-derived neurons in the olfactory bulb in EV-AP, WT-AP and K27M-AP. Scale bars represent 50 μ m. *p<0.05, **p<0.01, ****p<0.0001.

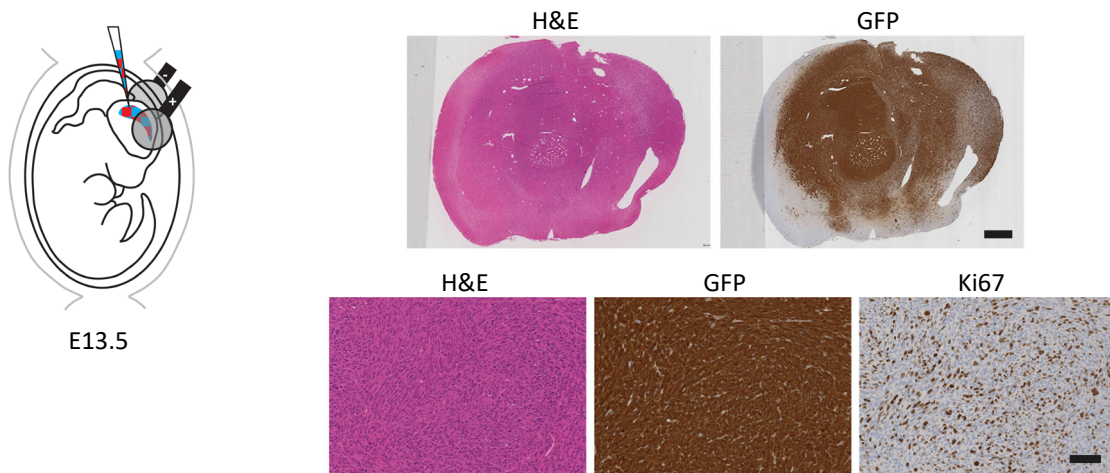
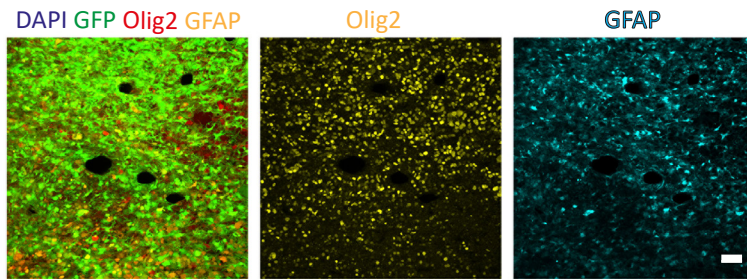
A**B**

Figure S3. Related to Figure 3. *In utero* delivery of piggyBac-transposable mutant PDGFRA^{D842V} along with knockdown of ATRX and p53 results in aggressive tumorigenesis and death by P28-P35, independent of H3.3^{K27M}. **(A)** Histology of mutant PDGFRA^{D842V}-driven GFP⁺ tumor containing Ki67⁺ cells. Scale bars represent 1 mm (top) and 100 μ m (bottom). **(B)** Mutant PDGFRA^{D842V}-driven tumors display both Olig2⁺ and GFAP⁺ cells. Scale bars represent 50 μ m.

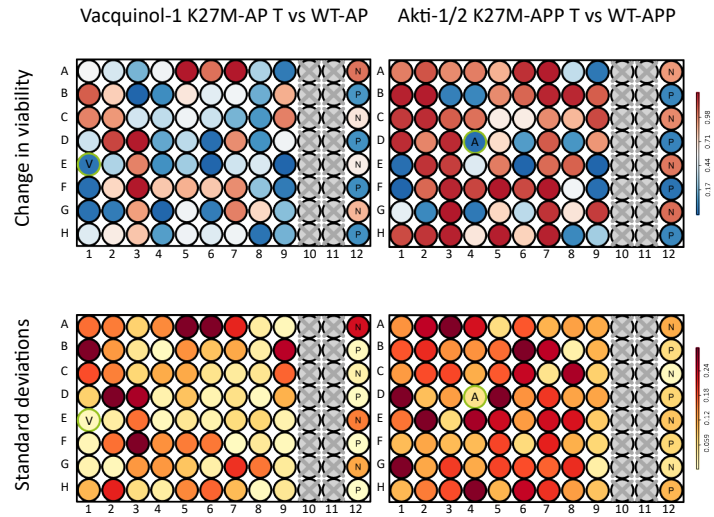
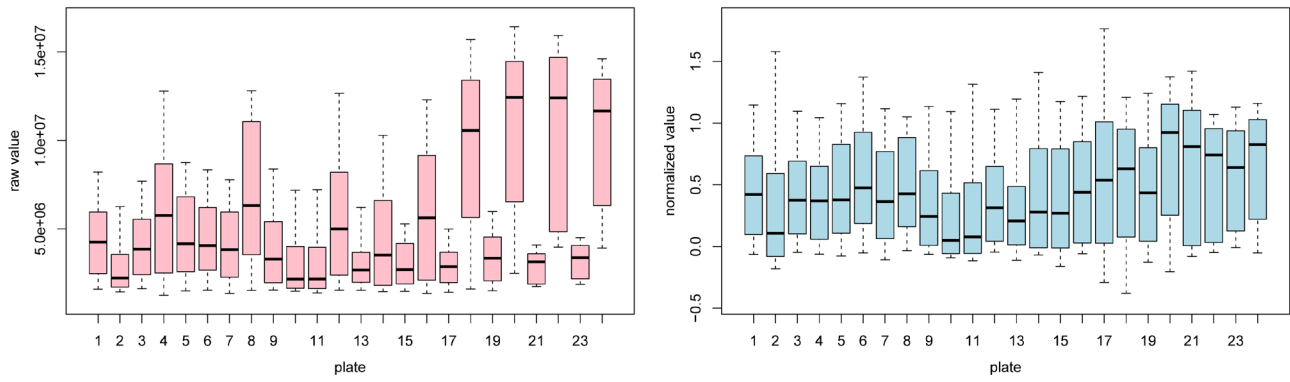
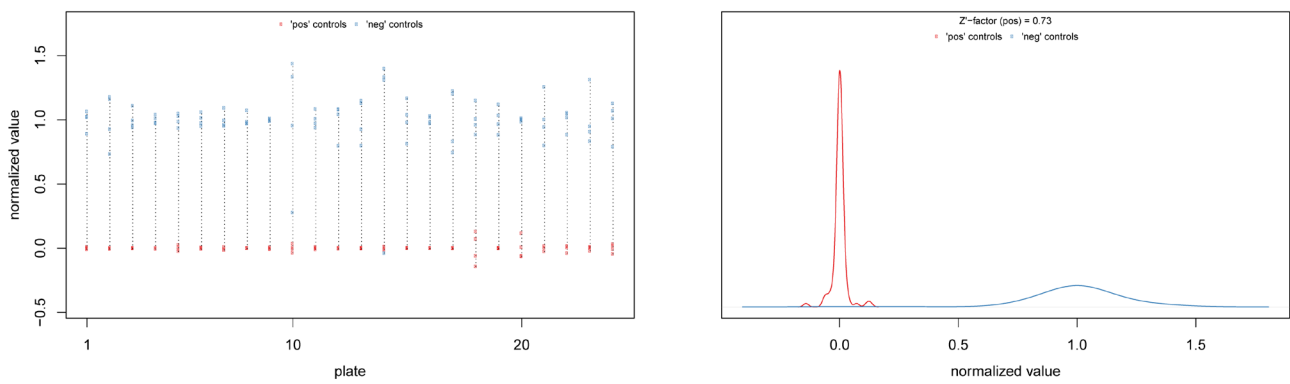
A**B****C**

Figure S4. Related to Figure 4. Targeted drug screen of K27M tumor cells using a small molecule library of 430 kinase inhibitors. (A) Viability change and standard deviations are shown for Vacquinol-1 responses in K27M-AP and Akti-1/2 responses in K27M-APP. Vacquinol-1 and Akti-1/2 wells are highlighted in green and with the letters “V” and “A”, respectively. “P” and “N” indicate positive and negative controls, respectively. **(B)** Distribution of raw (left panel) and normalized values (right panel) for all plates. The graphs show the median and variant distribution of signals in each plate. Each box displays the distribution of values based on minimum (low outlier), first quartile (low margin of box), median (line in the middle of the box), third quartile (top margin of box), and maximum (high outlier) of raw/normalized measured signals. **(C)** Distribution of controls in each plate. The left plot presents the signal from positive and negative controls at each plate and also the extension between positive control (Celecoxib indicated by red dots) and negative control (DMSO indicated by blue dots). The right plot shows the high Z'-factor (0.73) value, with another overview on positive and negative controls, obtained from kernel density estimates.

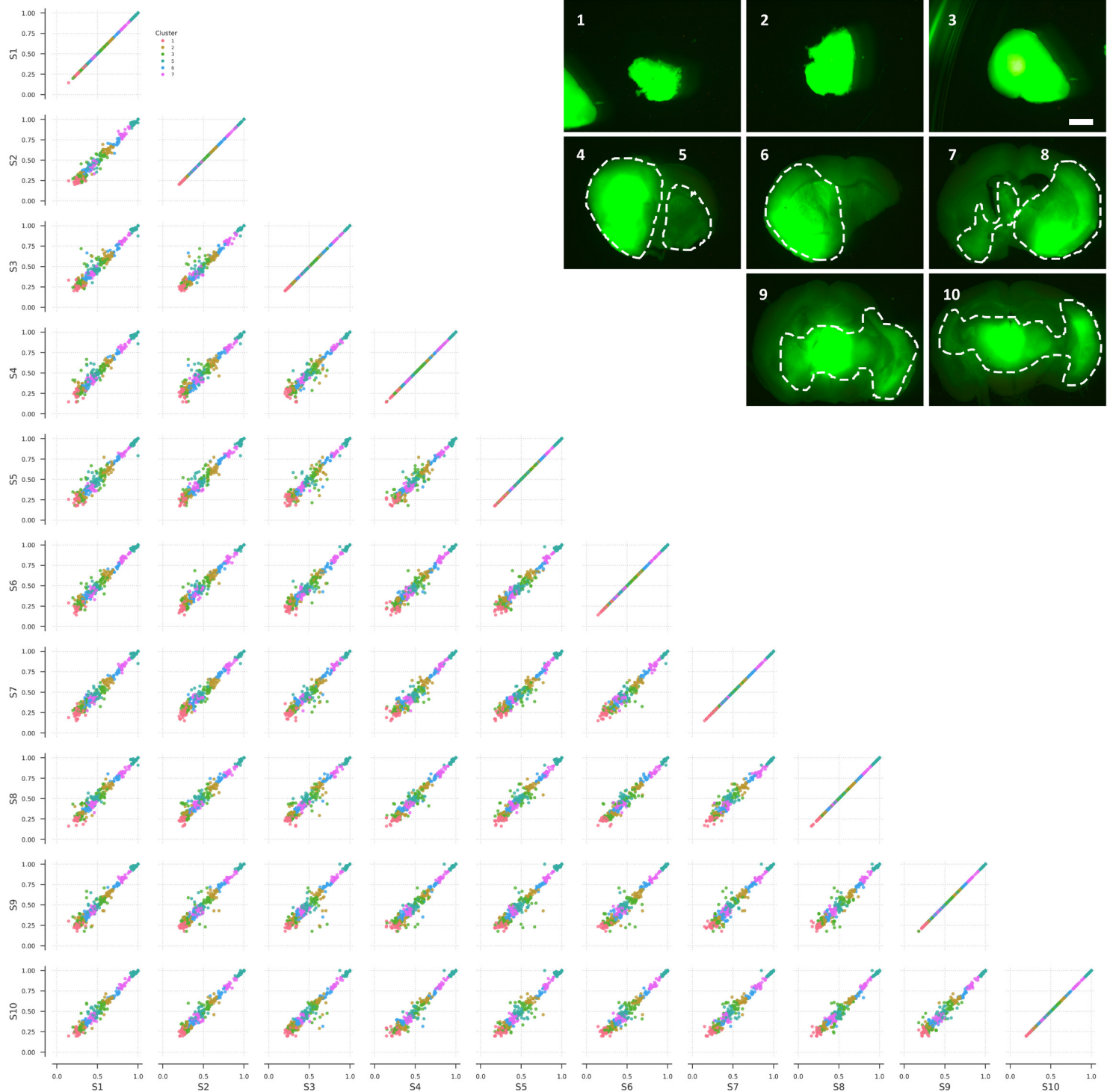
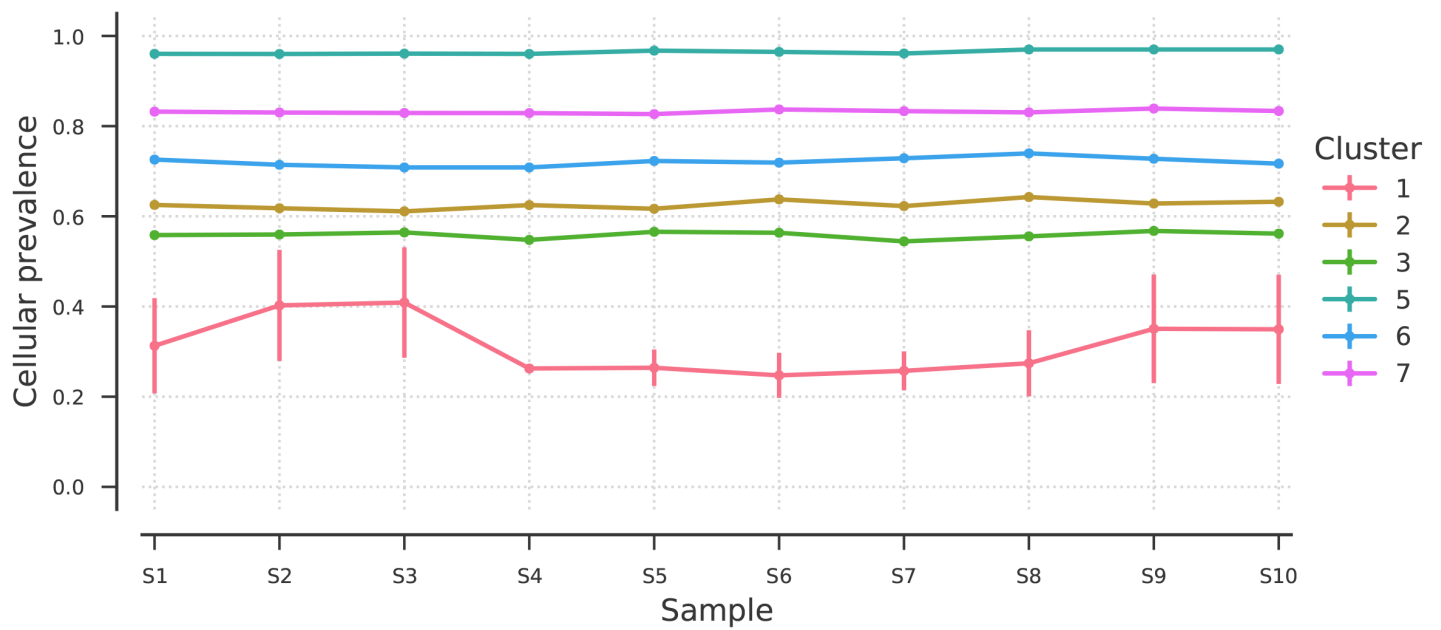
A**B**

Figure S5. Related to Figure 5. Homogeneity of the mutational landscape of 10 spatial biopsies of a K27M-AP tumor. (A) Clonality analysis of spatial biopsies of a K27M-AP tumor reveals 6 distinct clusters of SNVs. The set of SNVs used here are good-quality, non-synonymous SNVs that occur in gene exons. Each line corresponds to the cellular prevalence (y-axis) of each SNV cluster (identified by color) across the 10 spatial biopsies (x-axis). The error bars for each point indicate the standard deviation of the cellular prevalence of the constituent SNVs of each cluster in each biopsy. Inset shows GFP⁺ regions in the K27M-AP tumor used in this analysis. The regions shown within dashed lines were dissected for exome analysis. Scale bars represent 1.5 mm. **(B)** Comparisons of variant allele frequencies (VAF) of the constituent SNVs of the clusters determined in **(A)** between pairs of biopsies. Each point corresponds to an individual SNV, colored by the cluster to which it belongs, with its (x, y) coordinates representing its VAF in pairs of biopsies. Maximum concordance of VAFs appears as a $y = x$ line through the origin (shown here between the same biopsies). Error bars indicate the mean standard deviation of cellular prevalence estimates over all mutations in a cluster.

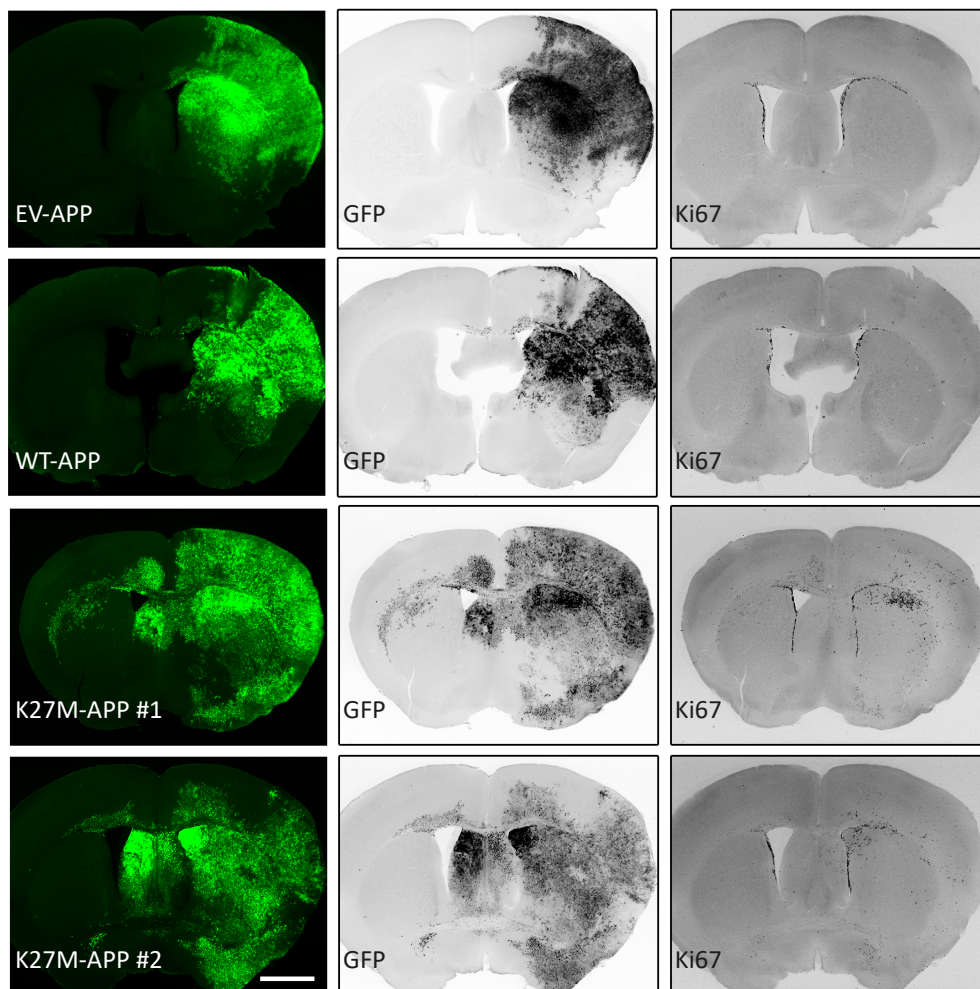
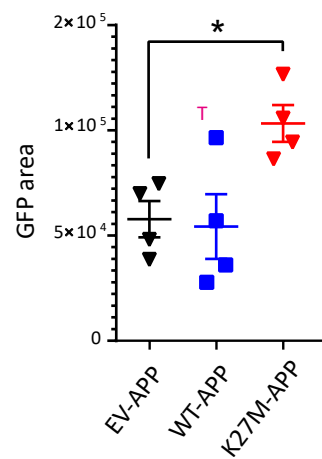
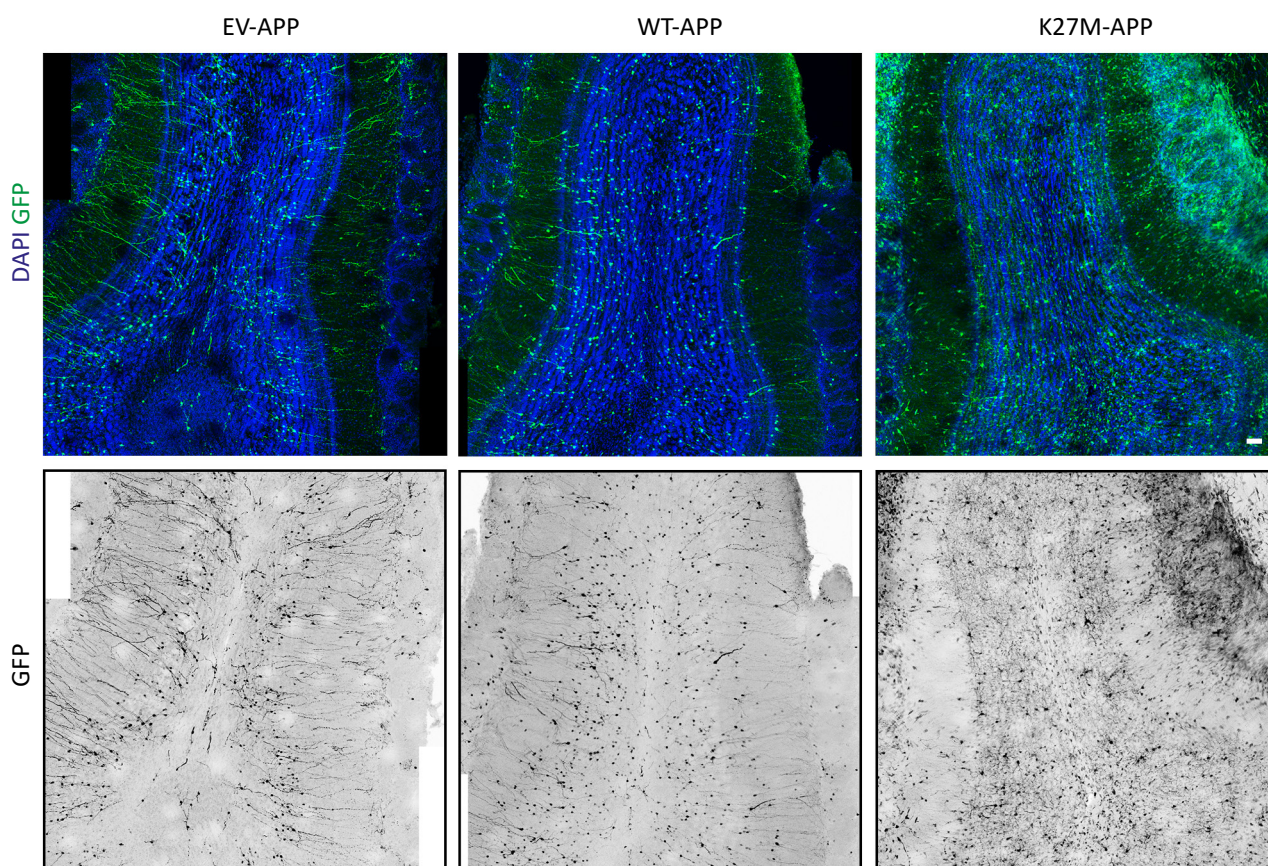
A**B****C**

Figure S6. Related to Figure 6. PDGFRA^{WT} overexpression increases the migration capacity of K27M-APP tumor cells and promotes a glial morphology or fate in the olfactory bulb. (A) Coronal sections demonstrating GFP⁺ signal in EV-APP, WT-APP and two different biological replicates of K27M-APP brains at 4 months following surgery. Scale bar represent 1.5 mm. **(B)** Quantification of total GFP⁺ area in EV-APP, WT-APP and K27M-APP coronal sections. One WT-APP low-penetrance tumor is marked “T”. Data are represented as mean \pm SEM. **(C)** Representative examples of number and morphology of subventricular zone (SVZ)-derived cells in the olfactory bulb in EV-APP, WT-APP and K27M-APP. Scale bar represent 50 μ m. *p<0.05, **p<0.01, ****p<0.0001.

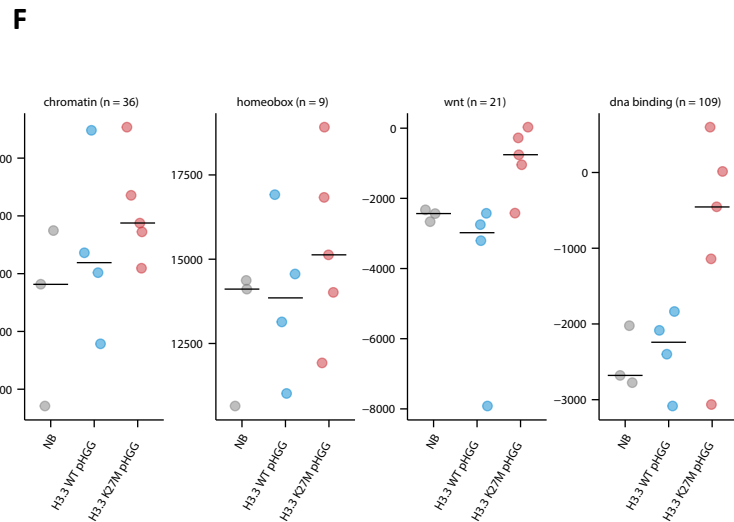
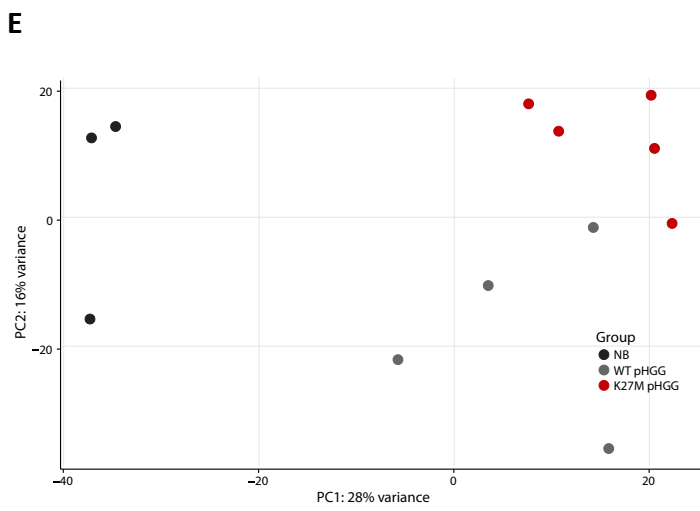
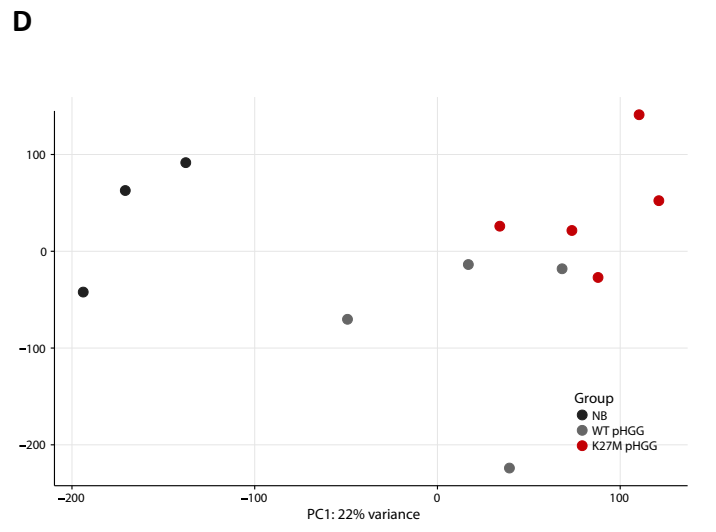
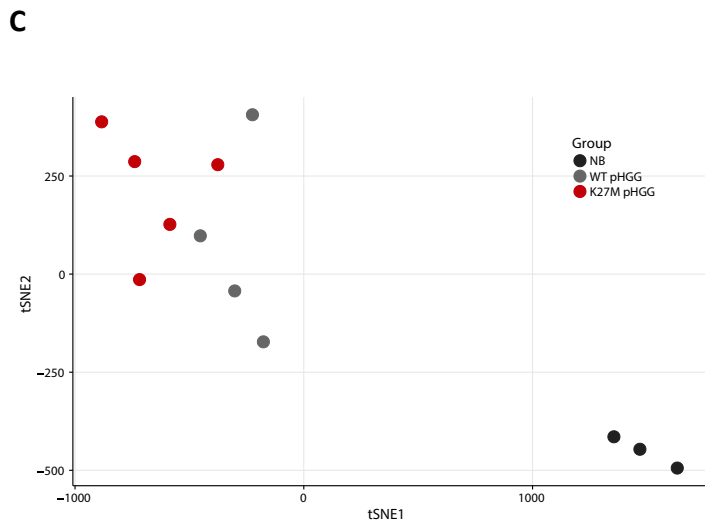
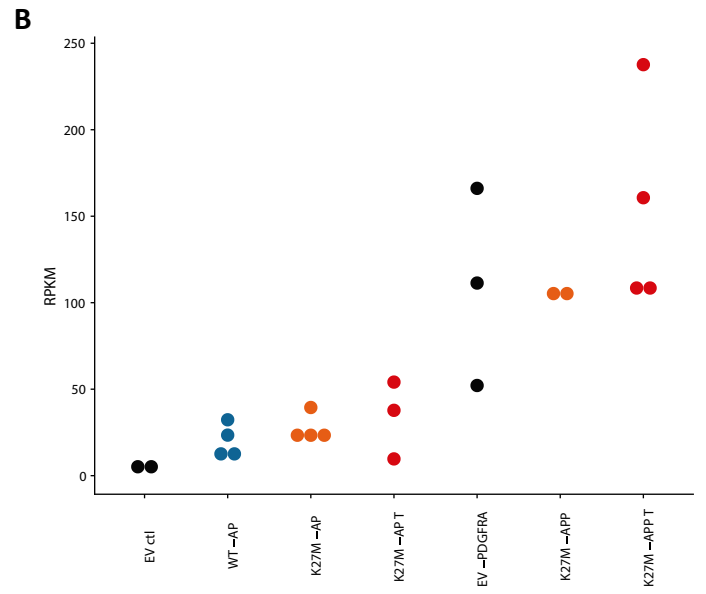
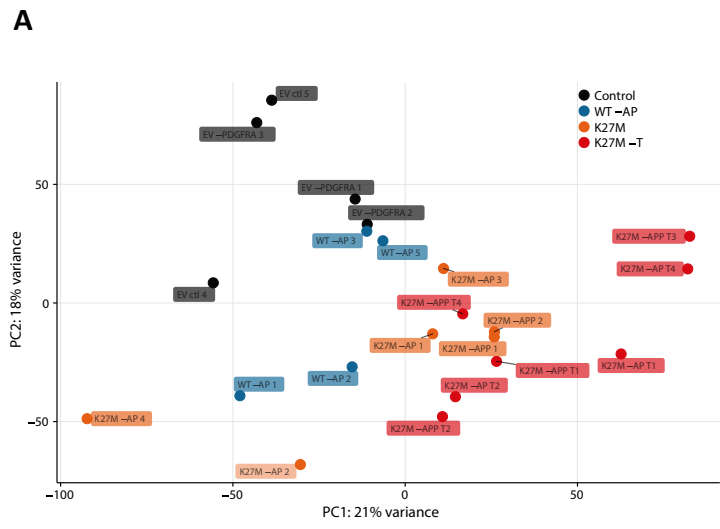


Figure S7. Related to Figure 7. H3.3^{K27M}-dependent transformation induces transcriptomic changes that are recapitulated in human tumors. (A) Principal component analysis (PCA) visualization of the murine samples based on transcriptome-wide expression level data. Black: EV ctl and EV PDGFRA. Blue: WT-AP. Orange: preneoplastic K27M cells (K27M). Red: K27M tumors (K27M-T). **(B)** Expression levels of *Pdgfra* across the cohort of RNA-Seq samples. RPKM values are reported here. **(C)** t-Embedded Neighbor Embedding (t-SNE) visualization of human samples based on the expression of the 870 most variant genes across human samples, illustrating the inferior separation of H3.3^{WT} and H3.3^{K27M} pHGG samples when human orthologs of the murine K27M-T signature (Figure 7A) are not used. Black: normal brain (NB). Grey: H3.3^{WT} pHGG. Red: H3.3^{K27M} pHGG. 10,000 iterations were performed on the PCA space (first 50 PCs) with perplexity=2, theta=0. Segregation of the three groups is specific to the K27M-T signature, and not obtained when using most variant genes (Figure 7B). **(D-E)** An analogous analysis of Figure 7C **(D)** and Figure S7C **(E)** using PCA visualization reveals the superior separation of H3.3^{WT} and H3.3^{K27M} pHGG samples through use of the human orthologs of the K27M-T signature. Black: normal brain (NB). Grey: H3.3^{WT} pHGG. Red: H3.3^{K27M} pHGG. **(F)** Genes specifically related to chromatin, homeobox, Wnt and DNA binding in the murine K27M-T signature are recapitulated in human H3.3^{K27M} pHGG (i.e. human tumors carrying H3.3^{K27M} mutations, *Trp53* loss-of-function mutations and moderate-to-high levels of *Pdgfra*). Reported here are the respective single-sample Gene Set Enrichment Analysis (ssGSEA) scores of each signature in human samples. Signature subsets were extracted from the murine K27M-AP complete signature using functional annotation with the DAVID tool (Table S7). Solid line: mean ssGSEA score per group.

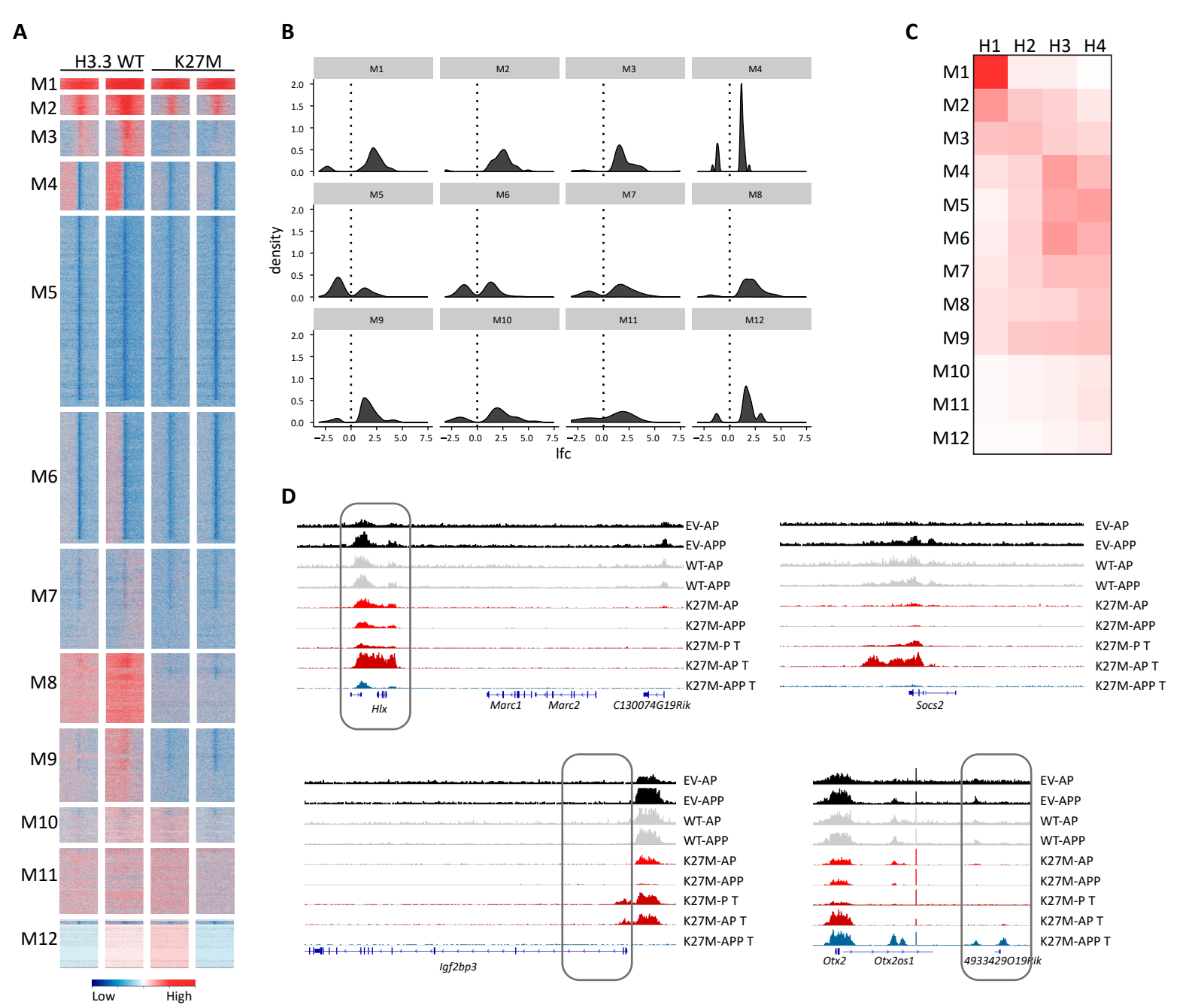


Figure S8. Related to Figure 8. K27M-induced alteration of genome-wide H3K27me3 deposition is captured by the mouse model. (A) Complete heatmap illustrating H3K27me3 levels at transcription start sites (TSSs) of all murine genes. H3K27me3 levels in regions of 10Kb surrounding TSSs (in rows) were normalized locally on a per-sample basis (in columns; from left-to-right: EV-ctl, EV-PDGFRA, K27M-AP T, K27M-APP T) and genes were subsequently clustered by k-means into k=12 clusters based on average perigenic H3K27me3 levels in each sample. Clusters M1-M4 consist of genes strongly regulated by H3K27me3; cluster M5 represents genes consistently depleted in the mark; and clusters M6 and upper M7 represent losses in H3K27me3 boundaries. The remaining clusters M8-M12 exhibit differing degrees of intra-cluster uniformity of H3K27me3 deposition and less consistently distinctive losses of the H3K27me3 along gene bodies. H3.3 WT: EV-ctl, EV-PDGFRA. K27M: K27M-AP T /K27M-APP T. **(B)** The distribution of changes in expression levels of deregulated genes in each of the clusters reveals a clear trend toward upregulation across most clusters (M1-M5, M8-M9, M12). Only significant gene expression changes are reported, in the form of \log_2 fold-change in K27M-T relative to baseline controls. **(C)** Pairwise similarity matrix between murine (rows) and human (columns; Figure 8C) gene clusters. Similarity was measured as the proportion of mouse genes with human orthologs present in each human cluster. While clusters M1-M5 exhibit more distinctive differences between H3.3^{WT} (EV-ctl and EV-PDGFRA) and H3.3^{K27M} (K27M-AP T, K27M-APP T) samples, clusters M6-M12 display variable degrees of recapitulation with human gene clusters. **(D)** *De novo* deposition of the H3K27me3 mark at the loci of *Hlx*, *Igf2bp3*, and *Socs2* in H3.3^{K27M}-tumors in spite of a global reduction in H3K27me3 levels. PDGFRA-independent increase in H3K27me3 levels that is specific to locus of *Hlx* but not to neighboring regions (see to the right). Increase in H3K27me3 levels in the promoter region of *Igf2bp3* in K27M-P T and K27M-AP T. Increase in H3K27me3 levels unique to K27M-AP T from the region upstream of *Socs2* followed by a loss of the mark when compared to controls (EV/WT-AP).